Available online at www.sciencedirect.com
ScienceDirect
Journal of Sound and Vibration 319 (2009) 1285–1300
JOURNAL OF SOUND AND VIBRATION
www.elsevier.com/locate/jsvi

# Underwater acoustic scattering from a radially layered cylindrical obstacle in a 3D ocean waveguide

A.M. Prospathopoulos[a,*], G.A. Athanassoulis[b], K.A. Belibassakis[c]

[a]*Hellenic Centre for Marine Research, Institute of Oceanography, 46.7 Km Athens-Sounio Avenue, P.O. Box 712, 190 13 Anavyssos, Greece*
[b]*National Technical University of Athens, School of Naval Architecture and Marine Engineering, Section of Ship and Marine Hydrodynamics, Heroon Polytechniou 9, 157 73 Athens, Greece*
[c]*Department of Naval Architecture, Technological Educational Institute of Athens, 122 10 Athens, Greece*

Received 10 January 2008; received in revised form 15 May 2008; accepted 30 June 2008
Handling Editor: C.L. Morfey
Available online 26 August 2008

**Abstract**

A solution based on coupled mode expansions is presented for the 3D problem of acoustic scattering from a radially layered penetrable cylindrical obstacle in a shallow-water plane-horizontal waveguide. Each cylindrical ring is characterized by a general, vertical sound speed and density profile (ssdp), the ocean environment around the obstacle can be also considered horizontally stratified with a depth-arbitrary ssdp, and the bottom is assumed to be rigid. The total acoustic field generated by an harmonic point source is represented as a normal-mode series expansion. The expansion coefficients are calculated exploiting the matching conditions at the cylindrical interfaces, which results in an infinite linear system. The system is appropriately truncated and numerically solved by using a recursive relation, which involves the unknown coefficients of two successive rings. Results concerning the transmission loss outside and inside obstacles consisting of three cylindrical rings are given for a typical depth-dependent ocean sound-speed profile. The presented solution can serve as a benchmark solution to the general problem of 3D acoustic scattering from axisymmetric inhomogeneities in ocean waveguides at low frequencies.


## 1. Introduction

During the last decades, a large number of both analytical and numerical methods have been developed dealing with the solution of acoustic propagation problems in ocean environments (see, for example, reviews [1,2]). The three-dimensional sound propagation and scattering in geometrically inhomogeneous ocean waveguides where backscattering is important (e.g. including obstacles or/and presenting steep bottom inhomogeneities) remains a subject of active research in underwater acoustics. The presence of strong discontinuities of the acoustic parameters in the horizontal direction renders most of the approximate techniques inapplicable, while the appropriate methods seems to be those which are based on the full-wave (Helmholtz) equation in conjunction with full matching conditions. Examples of these methods are

*Corresponding author. Tel.: +30 22910 76410; fax: +30 22910 76347.
*E-mail address:* aprosp@ath.hcmr.gr (A.M. Prospathopoulos).

0022-460X/$ - see front matter © 2008 Elsevier Ltd. All rights reserved.
doi:10.1016/j.jsv.2008.06.054

coupled-mode expansions, domain transformation techniques and boundary integral equations. Relevant references can be found in Refs. [3–6].

The present work focuses on the 3D scattering from azimuthally symmetric features by using the method of coupled modes. A first attempt concerning the treatment of the acoustic scattering from a penetrable cylindrical seamount using coupled modes has been undertaken by Evans [7], who extended his stepwise coupled-mode method [8] to three dimensions without providing numerical results. A relative work, using the coupled-mode approach but concerning elastic wave field computations, is that of Strange and Friederich [9], where scattering from a cylindrical elastic inclusion in a bounded elastic waveguide is considered. Based on Evans' works, coupled-mode solutions for the problem of 3D acoustic scattering from an axisymmetric seamount in shallow water have been presented for both impenetrable and penetrable cases [10,11]. Using a coupled mode method, Fawcett [12] presented results for 3D acoustic scattering from a finite cylinder in free space and embedded between two half-spaces, while more recently Athanassoulis et al. [13] studied the acoustic scattering from localized 3D scatterers. Recently, the problem of ambient noise scattering by a cylindrically symmetric seamount at low frequencies motivated Evans [14] to develop a stepwise coupled mode procedure for computing the total and scattered field, while an approach for modeling the scattering from azimuthally symmetric bathymetric features, appropriate for small mounds and indentations on the sea floor at high frequencies and seamounts, shoals and basins at low frequencies, is described in Ref. [15].

Analytical solutions to the above class of problems are always highly desirable, since they provide physical insight and serving as benchmarks for numerical methods and models. Such representative solutions can be found in Refs. [5,16–18]. Recently, Cai et al. [19] considered multiple scattering of acoustic waves in a planar horizontal waveguide by finite-length cylinders. This work, in which an analytically exact solution was obtained via the normal mode method for an isovelocity environment and scatterers with the same uniform properties, is focused on the comparison with the two-dimensional case, and especially on the band gap phenomenon and the mode interaction and mixing.

In the present work, which is a generalization of Refs. [5,18,20] to a more complex scattering configuration, numerical results are given for the 3D acoustic scattering from a cylindrically multi-layered, penetrable, island-type obstacle in an ocean waveguide with perfectly reflecting boundaries. The organization of the paper is the following. In Section 2 the mathematical formulation of the problem is described. In Section 3 the analytical solution of the problem concerning the 3D scattering from a single penetrable scatterer of constant acoustic properties in an isovelocity ocean waveguide is recalled. In Section 4 an infinite system of equations is derived for the unknown coefficients of the series expansions representing the pressure fields outside and inside the obstacle. In Section 5 numerical results concerning the transmission loss outside and inside cylindrical obstacles consisting of three radial layers are presented. The main features of the present work, conclusions and discussion are given in Section 6.

## 2. Mathematical formulation of the problem

Let us consider the following environment. A vertical cylindrical obstacle is surrounded by a horizontally stratified ocean of total constant depth $H$. The obstacle consists of $N-1$ concentric rings of external radius $r_j$, $j=1,\ldots,N-1$ (the number 1 denoting the inner cylinder and the number $N-1$ the outer cylindrical ring), and each one of them contains an arbitrary number of horizontal layers. The ocean waveguide is confined between a rigid (perfectly reflecting) bottom and a pressure-release sea surface. The cylindrical obstacle can be extended from the bottom up to the sea surface and all its interfaces are acoustically penetrable. The geometrical domains occupied by the acoustic materials in the $N-1$ rings and the surrounding water are denoted by $D^j$, $j=1,\ldots,N-1$, and $D^N$, respectively. Somewhere in $D^N$ a point source of unit strength is located, emitting monochromatic sound waves of angular frequency $\omega$. A cylindrical–polar coordinate system is introduced, with $z$-axis the axis of the cylinder pointing downward and origin at the intersection of $z$-axis with the sea surface. The source point is denoted by $\mathbf{r_s}=(r_s,z_s,0)$ and the generic field point is represented by $\mathbf{r}=(r,z,\theta)$. The acoustic properties (pressure $p$, sound speed $c$ and density $\rho$) of the media in the rings and the water are denoted with the subscripts $j=1,\ldots,N-1$, and $N$, respectively. The $(c,\rho)$-profiles in both water and cylindrical rings are assumed to be range independent, that is $c_j=c_j(z)$ and $\rho_j=\rho_j(z)$, $j=1,\ldots,N-1$. For the environment described above the cross-section passing through the source and the axis of the obstacle

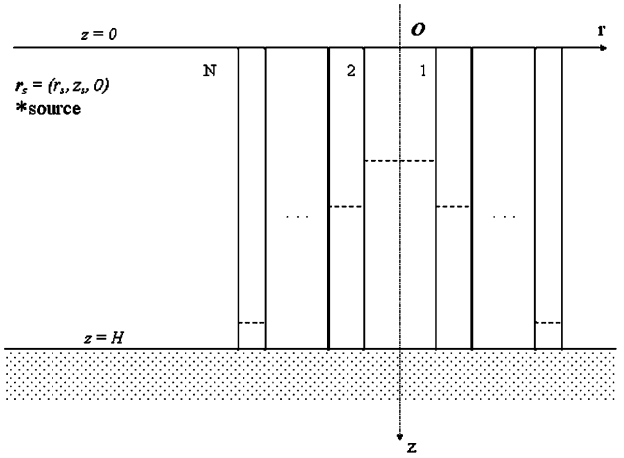


Fig. 1. The geometrical configuration of the studied environment at a cross-section passing through the source and the axis of the cylindrical obstacle.

is depicted in Fig. 1. The acoustic propagation/scattering problem for the total pressure field in the above environment is governed by the Helmholtz equations

$$\nabla_\rho^2 p_j + k_j^2(z) p_j = 0, \quad \mathbf{r} \in D^j, \ j = 1, \ldots, N-1, \tag{1}$$

$$\nabla_\rho^2 p_N + k_N^2(z) p_N = -\frac{\delta(r - r_s)\delta(z - z_s)\delta(\theta)}{r}, \quad \mathbf{r_s}, \mathbf{r} \in D^N, \tag{2}$$

accompanied by the boundary conditions at the surface and the bottom of the waveguide

$$p_j = 0, \quad z = 0, \ j = 1, \ldots, N, \tag{3a}$$

$$\frac{\partial p_j}{\partial z} = 0, \quad z = H, \ j = 1, \ldots, N \tag{3b}$$

and the matching conditions expressing continuity of pressure and normal velocity at the cylindrical interfaces

$$p_j = p_{j+1}, \quad r = r_j, \ j = 1, \ldots, N-1, \tag{4a}$$

$$\frac{1}{\rho_j(z)} \frac{\partial p_j}{\partial r} = \frac{1}{\rho_{j+1}(z)} \frac{\partial p_{j+1}}{\partial r}, \quad r = r_j, \ j = 1, \ldots, N-1. \tag{4b}$$

Possible horizontal stratification in the cylindrical rings and the surrounding water introduces additionally to the formulation conditions of continuity of pressure and normal velocity at the horizontal interfaces, similar to Eqs. (4a) and (4b). An appropriate (Sommerfeld) radiation condition, expressing that the pressure field at infinity ($r \longrightarrow \infty$) behaves like a system of cylindrical outgoing waves, completes the mathematical formulation of the studied problem.

In the above equations $p_j = p_j(r, z, \theta)$ is the complex amplitude of the acoustic pressure in $D^j$, the time harmonic dependence $e^{-i\omega t}$ being factored out, the Laplacian operator $\nabla_\rho^2$ is given by

$$\nabla_\rho^2 = \frac{1}{r}\frac{\partial}{\partial r}\left(r\frac{\partial}{\partial r}\right) + \rho\frac{\partial}{\partial z}\left(\frac{1}{\rho}\frac{\partial}{\partial z}\right) + \frac{1}{r^2}\frac{\partial^2}{\partial \theta^2}, \tag{5}$$

and $k_j(z) = \omega/c_j(z), j = 1, \ldots, N-1$, $k_N(z) = \omega/c_N(z)$ are the wavenumbers in the $N-1$ cylindrical rings and the water, respectively.

## 3. The solution for the single penetrable scatterer

Before proceeding to the treatment of the problem formulated in the previous section, the analytical solution of the problem concerning the 3D scattering from a single penetrable scatterer of constant acoustic properties $(c_b, \rho_b)$ in an isovelocity horizontal ocean waveguide (with constant $c_w, \rho_w$) will be recalled. In this case, $N=2$ and $r_1=a$ is the radius of the single cylindrical scatterer. According to Ref. [18], Eq. (24), the total pressure field outside the cylindrical scatterer, $p_w$, is represented as the sum of an axisymmetric incident field $p_i$ (the field generated by a point source in the unobstructed waveguide) and a scattered field, $p_w^{sc}$, as follows:

$$p_w(r,z,\theta)=p_i+p_w^{sc}=\frac{i}{4\rho(z_s)}\sum_{n=1}^{\infty}g_n(z_s)H_0^{(1)}(\lambda_n R)g_n(z)+\sum_{n=1}^{\infty}g_n(z_s)g_n(z)\sum_{m=0}^{\infty}e_m A_{nm}^{sc}H_m^{(1)}(\lambda_n r_s)\widetilde{H}_m^{(1)}(\lambda_n r)\cos m\theta, \tag{6}$$

where the coefficients $A_{nm}^{sc}$ are given as

$$A_{nm}^{sc}=-\frac{1}{\rho(z_s)}\left[\frac{J_m(\mu_n a)}{2\pi D_{nm}}+\frac{i}{4}J_m(\lambda_n a)\right] \tag{7}$$

and

$$D_{nm}=\lambda_n a J_m(\mu_n a)H_m^{(1)'}(\lambda_n a)-\gamma\mu_n a J_m'(\mu_n a)H_m^{(1)}(\lambda_n a). \tag{8}$$

Also, according to Ref. [18], Eq. (23), the pressure field inside the scatterer, $p_b$, is expressed as

$$p_b=-\sum_{n=1}^{\infty}g_n(z_s)\psi_n(z)\sum_{m=0}^{\infty}e_m\left[\frac{\sqrt{\gamma}}{2\pi\rho(z_s)D_{nm}}\right]H_m^{(1)}(\lambda_n r_s)J_m(\mu_n r)\cos m\theta. \tag{9}$$

In the above equations, $\lambda_n$, $\mu_n$ are the eigenvalues and $g_n(z)$, $\psi_n(z)$ are the normalized eigenfunctions of the normal Sturm–Liouville eigenvalue problem (called hereafter as *vertical eigenvalue problem*), outside and inside the scatterer, respectively, obtained from Eqs. (1), (3a) and (3b) after separation of variables, $\gamma=\rho_w/\rho_b$, $e_0=1$, $e_m=2$, $m>0$, $R=(r_s^2+r^2-2r_s r\cos\theta)^{1/2}$ is the distance between the source and the field point, $a$ is the radius of the scatterer, and $J_m(\cdot)$, $H_m^{(1)}(\cdot)$ are the $m$-th-order Bessel and first kind Hankel functions. The prime denotes differentiation with respect to the argument and $\widetilde{H}_m^{(1)}(\cdot)$ are the normalized Hankel functions $H_m^{(1)}(\cdot)/H_m^{(1)}(\lambda_n a)$.

We note here that the above normal mode expansions are valid for all values of $k_j a$, $j=1,2$. However, it is well known that for large values of $k_j a$ the $m$-summation in Eqs. (6) and (9) is quite laborious, since many azimuthal terms have to be retained in order for the corresponding series to converge. A study of the azimuthal convergence of this series in the simple case of impenetrable soft/hard vertical inclusion is presented in Ref. [21], where results up to $ka\simeq 1000$ were obtained. Specifically, for $k_j a\geqslant 1$, the creeping wave series obtained from the above equations by applying Sommerfeld–Watson transformation techniques (see, for example, Refs. [22,23]) can be used in order for the series to converge substantially faster, especially in the shadow zone behind the vertical cylinder. Such an application needs particular investigation and it is left to be carried out in a future work.

## 4. Series expansion of the acoustic pressure

Applying the method of separation of variables and decomposing the total pressure fields inside and outside the cylindrical obstacle into the incident field and the scattered field, the acoustic field in the cylindrical rings, $p_1$, $\{p_j,\ j=2,\ldots,N-1\}$, and the surrounding water, $p_N$, can be written in the form of normal-mode series expansions as follows (see also Refs. [5,18]):

$$p_1(r,z,\theta)=\sum_{n=1}^{\infty}g_n^1(z)\sum_{m=0}^{\infty}e_m d_{s,nm}A_{nm}^1\overline{J}_{nm}^1(r)\cos m\theta, \tag{10}$$

$$p_j(r,z,\theta)=\sum_{n=1}^{\infty} g_n^j(z)\sum_{m=0}^{\infty} e_m d_{s,nm}[A_{nm}^j \overline{H1}_{nm}^j(r)+B_{nm}^j \overline{H2}_{nm}^j(r)]\cos m\theta,\quad j=2,\ldots,N-1, \tag{11}$$

$$p_N(r,z,\theta)=\sigma\sum_{n=1}^{\infty} g_n^N(z_s)H_0^{(1)}(\lambda_n^N R)g_n^N(z)+\sum_{n=1}^{\infty} g_n^N(z)\sum_{m=0}^{\infty} e_m d_{s,nm}A_{nm}^N \overline{H1}_{nm}^N(r)\cos m\theta, \tag{12}$$

where

$$\sigma=\frac{i}{4\rho(z_s)}, \tag{13}$$

$$d_{s,nm}=H_m^{(1)}(\lambda_n^N r_s)g_n^N(z_s), \tag{14}$$

$$\overline{H1}_{nm}^j(r)=\frac{H_m^{(1)}(\lambda_n^j r)}{H_m^{(1)}(\lambda_n^j r_j)}, \tag{15a}$$

$$\overline{H2}_{nm}^j(r)=\frac{H_m^{(2)}(\lambda_n^j r)}{H_m^{(2)}(\lambda_n^j r_j)}, \tag{15b}$$

$$\overline{J}_{nm}^j(r)=\frac{J_m(\lambda_n^j r)}{J_m(\lambda_n^j r_j)}, \tag{15c}$$

$\lambda_n^j$ are the eigenvalues and $g_n^j(z)$ the normalized eigenfunctions of the vertical eigenvalue problem in the $j$ cylindrical ring, $H_m^{(2)}(\lambda_n^j r)$ are the $m$-th-order second kind Hankel functions, and $\{A_{nm}^j,\ j=1,\ldots,N\}$ and $\{B_{nm}^j,\ j=2,\ldots,N-1\}$ are appropriate constants to be determined. All other coefficients and quantities have been defined in Section 3. Hankel functions of the second kind in Eq. (11) model the incoming waves in the intermediate rings $2,\ldots,N-1$. Note that, in the special case $j=N$ we consider $r_j=r_{N-1}$.

As can be seen from Eqs. (15a)–(15c), the pressure field is formulated using scaled Hankel and Bessel functions relative to a nearby interface in order to avoid numerical overflow problems, associated with the phenomenon of exponential dichotomy (see also Section 5.1).

Exploiting the matching conditions (4a) and (4b), linear systems of equations are obtained, permitting the calculation of the coefficients $A_{nm}^j$ and $B_{nm}^j$. Before proceeding to the construction of these systems, we recall the orthonormality conditions for the vertical eigenfunctions $\{g_n^j(z),\ j=1,\ldots,N\}$

$$\int_0^H \frac{1}{\rho_j(z)} g_n^j(z)g_v^j(z)\,\mathrm{d}z=\begin{cases}1, & n=v,\\ 0, & n\neq v\end{cases} \tag{16}$$

and the Graf's addition theorem for the Hankel functions (see, e.g., Ref. [24])

$$H_0^{(1)}(\lambda_n R)=\sum_{m=0}^{\infty} e_m H_m^{(1)}(\lambda_n r_s)J_m(\lambda_n r)\cos m\theta. \tag{17}$$

We start with the implementation of the matching conditions for two intermediate cylindrical rings. Substituting Eq. (11) into Eqs. (4a) and (4b), and using property (16) and the orthonormality of the azimuthal eigenfunctions $\cos m\theta$, we obtain the following system of equations:

$$A_{vm}^j+B_{vm}^j=\sum_{n=1}^{\infty}\widetilde{\mathscr{C}}_{vn,m}^{j,j+1}\left[A_{nm}^{j+1}\overline{H1}_{nm}^{j+1}(r_j)+B_{nm}^{j+1}\overline{H2}_{nm}^{j+1}(r_j)\right], \tag{18a}$$

$$A_{vm}^j q_{vm}^{1,j}(r_j)+B_{vm}^j q_{vm}^{2,j}(r_j)=\sum_{n=1}^{\infty}\widetilde{\mathscr{C}}_{vn,m}^{j,j+1}\left[A_{nm}^{j+1}\overline{Q1}_{nm}^{j+1}(r_j)+B_{nm}^{j+1}\overline{Q2}_{nm}^{j+1}(r_j)\right], \tag{18b}$$

where

$$\widetilde{\mathscr{C}}^{j,j+1}_{vn,m} = \frac{d_{s,nm}}{d_{s,vm}}\tilde{c}^{j,j+1}_{vn}, \tag{19a}$$

$$\widetilde{\mathscr{C}}^{j,j+1}_{vn,m} = \frac{d_{s,nm}}{d_{s,vm}}\hat{c}^{j,j+1}_{vn}, \tag{19b}$$

$$q^{\ell,j}_{nm}(r) = \frac{H^{(\ell)'}_m(\lambda^j_n r)}{H^{(\ell)}_m(\lambda^j_n r)}, \quad \ell = 1,2, \tag{20}$$

$$\overline{Q1}^{j+1}_{nm}(r_j) = q^{1,j+1}_{nm}(r_j)\overline{H1}^{j+1}_{nm}(r_j), \tag{21a}$$

$$\overline{Q2}^{j+1}_{nm}(r_j) = q^{2,j+1}_{nm}(r_j)\overline{H2}^{j+1}_{nm}(r_j). \tag{21b}$$

In the above equations (19), the quantities

$$\tilde{c}^{j,j+1}_{vn} = \int_0^H \frac{1}{\rho_j(z)} g^{j+1}_n(z) g^j_v(z)\,\mathrm{d}z, \tag{22a}$$

$$\hat{c}^{j,j+1}_{vn} = \frac{\lambda^{j+1}_n}{\lambda^j_v}\int_0^H \frac{1}{\rho_{j+1}(z)} g^{j+1}_n(z) g^j_v(z)\,\mathrm{d}z, \tag{22b}$$

are the coupling coefficients expressing the interchange of energy between the cylindrical rings. Both vertical modes and the corresponding projection integrals in Eqs. (22) are independent of the azimuthal order $m$, and thus, they are calculated only once for each value of vertical index $n$ in each cylindrical subdomain $D^j$; see Fig. 1. The function $H^{(\ell)'}_m(\lambda^j_n r)$ appearing in Eq. (20) denotes the first derivative of the corresponding Hankel function with respect to the argument.

System (18a) and (18b) allows the coefficients $A^j_{nm}$, $B^j_{nm}$ to be expressed in terms of $A^{j+1}_{nm}$, $B^{j+1}_{nm}$ as follows:

$$A^j_{vm} = \sum_{n=1}^{\infty} \mathscr{E}^{\mathrm{I},j}_{vn,m}(r_j) A^{j+1}_{vm} + \sum_{n=1}^{\infty} \mathscr{E}^{\mathrm{II},j}_{vn,m}(r_j) B^{j+1}_{vm}, \tag{23a}$$

$$B^j_{vm} = \sum_{n=1}^{\infty} \mathscr{E}^{\mathrm{III},j}_{vn,m}(r_j) A^{j+1}_{vm} + \sum_{n=1}^{\infty} \mathscr{E}^{\mathrm{IV},j}_{vn,m}(r_j) B^{j+1}_{vm}, \tag{23b}$$

where

$$\mathscr{E}^{i,j}_{vn,m}(r_j) = S\frac{q^{\ell,j}_{vm}(r_j)\widetilde{\mathscr{C}}^{j,j+1}_{vn,m}\overline{H\kappa}^{j+1}_{nm}(r_j) - \widetilde{\mathscr{C}}^{j,j+1}_{vn,m}\overline{Q\kappa}^{j+1}_{nm}(r_j)}{\Delta q^j_{vm}(r_j)}, \tag{24}$$

$$\Delta q^j_{vm}(r_j) = q^{2,j}_{vm}(r_j) - q^{1,j}_{vm}(r_j) = \frac{H^{(2)}_{m-1}(\lambda^j_v r_j)}{H^{(2)}_m(\lambda^j_v r_j)} - \frac{H^{(1)}_{m-1}(\lambda^j_v r_j)}{H^{(1)}_m(\lambda^j_v r_j)}. \tag{25}$$

The triplet $(S,\ell,\kappa)$ takes the values $(1,2,1)$ for $i=\mathrm{I}$, $(1,2,2)$ for $i=\mathrm{II}$, $(-1,1,1)$ for $i=\mathrm{III}$, and $(-1,1,2)$ for $i=\mathrm{IV}$.

We proceed with the implementation of the matching condition for the first (inner) cylindrical interface. Substituting Eqs. (10), (11) into Eqs. (4a) and (4b), and working similarly with the case of the two intermediate cylindrical rings, we obtain

$$A^1_{vm} = \sum_{n=1}^{\infty} \mathscr{E}^{\mathrm{I},1}_{vn,m}(r_1) A^2_{vm} + \sum_{n=1}^{\infty} \mathscr{E}^{\mathrm{II},1}_{vn,m}(r_1) B^2_{vm}, \tag{26a}$$

$$0 = \sum_{n=1}^{\infty} \mathscr{E}^{\mathrm{III},1}_{vn,m}(r_1) A^2_{vm} + \sum_{n=1}^{\infty} \mathscr{E}^{\mathrm{IV},1}_{vn,m}(r_1) B^2_{vm}. \tag{26b}$$

where

$$\mathscr{E}^{\mathrm{I},1}_{vn,m}(r_1) = \widetilde{\mathscr{C}}^{1,2}_{vn,m}\overline{H1}^2_{nm}(r_1), \tag{27a}$$

$$\mathscr{E}^{\mathrm{II},1}_{vn,m}(r_1) = \widetilde{\mathscr{C}}^{1,2}_{vn,m}\overline{H2}^2_{nm}(r_1), \tag{27b}$$

$$\mathscr{E}^{\mathrm{III},1}_{vn,m}(r_1) = \widetilde{\mathscr{C}}^{1,2}_{vn,m}\overline{H1}^2_{nm}(r_1) - p_{vm}(r_1)\widetilde{\mathscr{C}}^{1,2}_{vn,m}\overline{Q1}^2_{nm}(r_1), \tag{27c}$$

$$\mathscr{E}^{\mathrm{IV},1}_{vn,m}(r_1) = \widetilde{\mathscr{C}}^{1,2}_{vn,m}\overline{H2}^2_{nm}(r_1) - p_{vm}(r_1)\widetilde{\mathscr{C}}^{1,2}_{vn,m}\overline{Q2}^2_{nm}(r_1), \tag{27d}$$

and

$$p_{vm}(r_1) = \frac{J_m(\lambda^1_v r_1)}{J'_m(\lambda^1_v r_1)}. \tag{28}$$

Finally, in order to implement the matching condition for the last (outer) cylindrical interface, we substitute expressions (11) and (12) into Eqs. (4a) and (4b) and take into account Graf's theorem (Eq. (17)). Working similarly with the above two cases we obtain

$$A^{N-1}_{vm} = \sum_{n=1}^{\infty}\mathscr{E}^{\mathrm{I},N-1}_{vn,m}(r_{N-1})A^N_{vm} + \sum_{n=1}^{\infty}\mathscr{E}^{\mathrm{II},N-1}_{vn,m}(r_{N-1})B^N_{vm}, \tag{29a}$$

$$B^{N-1}_{vm} = \sum_{n=1}^{\infty}\mathscr{E}^{\mathrm{III},N-1}_{vn,m}(r_{N-1})A^N_{vm} + \sum_{n=1}^{\infty}\mathscr{E}^{\mathrm{IV},N-1}_{vn,m}(r_{N-1})B^N_{vm}, \tag{29b}$$

where the coefficients $\mathscr{E}^{i,N-1}_{vn,m}(r_{N-1})$ can be calculated from Eqs. (24) and (25), setting

$$\overline{H1}^N_{nm}(r_{N-1}) = 1, \quad i = \mathrm{I}, \mathrm{III}, \tag{30a}$$

$$\overline{H2}^N_{nm}(r_{N-1}) = \sigma J_m(\lambda^N_n r_{N-1}), \quad i = \mathrm{II}, \mathrm{IV}, \tag{30b}$$

$$\overline{Q2}^N_{nm}(r_{N-1}) = \sigma J'_m(\lambda^N_n r_{N-1}), \quad i = \mathrm{II}, \mathrm{IV}. \tag{30c}$$

Eqs. (23a), (23b), (26a), (26b) and (29a), (29b) constitute an infinite system, called the system $\mathscr{S}$, which has to be solved for $\{A^j_{vm}, j = 1, \ldots, N\}$ and $\{B^j_{vm}, j = 2, \ldots, N-1\}$. Observing the aforementioned equations one can note that the azimuthal index $m$ serves as an independent parameter, i.e. system $\mathscr{S}$ can be solved for each $m$ independently, as in the case of a single cylindrical penetrable obstacle [18]. In the course of the numerical calculations the system $\mathscr{S}$ for each $m$ is truncated to a finite one, retaining only $n = n_w$ terms (see Section 5.1). Thus, the finite system for a fixed $m$ can be written in a matrix form as follows:

$$\begin{bmatrix} \mathbf{a}^j \\ \mathbf{b}^j \end{bmatrix} = \begin{bmatrix} \mathbf{E}^{\mathrm{I},j} & \mathbf{E}^{\mathrm{II},j} \\ \mathbf{E}^{\mathrm{III},j} & \mathbf{E}^{\mathrm{IV},j} \end{bmatrix} \begin{bmatrix} \mathbf{a}^{j+1} \\ \mathbf{b}^{j+1} \end{bmatrix}, \tag{31}$$

where

$$\mathbf{a}^j = \begin{bmatrix} A^j_{1m} \\ \vdots \\ A^j_{n_w m} \end{bmatrix}, \quad \mathbf{b}^j = \begin{bmatrix} B^j_{1m} \\ \vdots \\ B^j_{n_w m} \end{bmatrix}, \ j = 1, \ldots, N, \tag{32a}$$

$$\mathbf{E}^{i,j} = \begin{bmatrix} \mathscr{E}^{i,j}_{11}(r_j) & \cdots & \mathscr{E}^{i,j}_{1n_w}(r_j) \\ \vdots & \ddots & \vdots \\ \mathscr{E}^{i,j}_{n_w 1}(r_j) & \cdots & \mathscr{E}^{i,j}_{n_w n_w}(r_j) \end{bmatrix}, \quad j = 1, \ldots, N, \ \ i = \mathrm{I}, \ldots, \mathrm{IV}, \tag{32b}$$

taking into account that

$$\mathbf{b}^1 = \mathbf{0}, \tag{33a}$$

$$\mathbf{b}^N = \mathbf{1}. \tag{33b}$$

Repeated application of the recursive relation (31) yields

$$\begin{bmatrix} \mathbf{a}^1 \\ \mathbf{b}^1 \end{bmatrix} = \begin{bmatrix} \mathbf{R}^{\mathrm{I}} & \mathbf{R}^{\mathrm{II}} \\ \mathbf{R}^{\mathrm{III}} & \mathbf{R}^{\mathrm{IV}} \end{bmatrix} \begin{bmatrix} \mathbf{a}^N \\ \mathbf{b}^N \end{bmatrix}, \tag{34}$$

where

$$\begin{bmatrix} \mathbf{R}^{\mathrm{I}} & \mathbf{R}^{\mathrm{II}} \\ \mathbf{R}^{\mathrm{III}} & \mathbf{R}^{\mathrm{IV}} \end{bmatrix} = \begin{bmatrix} \mathbf{E}^{\mathrm{I},1} & \mathbf{E}^{\mathrm{II},1} \\ \mathbf{E}^{\mathrm{III},1} & \mathbf{E}^{\mathrm{IV},1} \end{bmatrix} \cdots \begin{bmatrix} \mathbf{E}^{\mathrm{I},N-1} & \mathbf{E}^{\mathrm{II},N-1} \\ \mathbf{E}^{\mathrm{III},N-1} & \mathbf{E}^{\mathrm{IV},N-1} \end{bmatrix}. \tag{35}$$

Combination of Eqs. (33a), (33b) and (34) implies

$$\mathbf{a}^1 = \mathbf{R}^{\mathrm{I}}\mathbf{a}^N + \mathbf{R}^{\mathrm{II}}\mathbf{1} \tag{36a}$$

$$\mathbf{0} = \mathbf{R}^{\mathrm{III}}\mathbf{a}^N + \mathbf{R}^{\mathrm{IV}}\mathbf{1} \tag{36b}$$

Matrix $\mathbf{a}^N$ is calculated from Eq. (36b) and then, taking into account Eq. (33b), matrices $\mathbf{a}^j$ and $\mathbf{b}^j$ are calculated by backward use of the recursion relation (31). Note that the values of $\mathbf{b}^1$, computed using Eq. (34), should be sufficiently close to zero, while their magnitudes serve as an indicator for the success of solving Eq. (36b).

The analysis presented above has been verified against the analytical solution of a simplified propagation/scattering problem, which is described in the Appendix.

## 5. Numerical results

In this section, numerical aspects of the studied problem are considered and low-frequency results demonstrating the 3D effects of a radially-layered cylindrical obstacle in an ocean waveguide are presented. The numerical examples illustrated herein are representative of the multi-parametric character of the problem and the complexity of the provided solution.

### 5.1. Numerical considerations

The general analysis made in Ref. [18] concerning the truncation of the $n$ vertical terms in the sum of the pressure field for the problem of 3D scattering from a single cylindrical obstacle also applies to the problem of a radially layered cylindrical structure. In the numerical examples of this section the pressure field has been calculated by retaining only the propagating modes, i.e. the terms corresponding to real positive eigenvalues of the vertical eigenvalue problem. Furthermore, their number is the same throughout the cylindrical rings of the scatterer and the water column due to the low frequency of the studied environment.

As concerns the truncation of the $m$ azimuthal terms in the sum of the pressure field, the same number of terms, $m_{\max}$, was used globally (i.e. throughout the obstacle and the surrounding water) in order to achieve convergence of the double series expressing the scattered field outside the obstacle and the total field inside the obstacle. Following the rationale of works [18,21], a lower bound of $m_{\max}$ is derived by imposing $m_{\max} > m_{cr}^N(n=1) = \lambda_1^N r_N$, where $m_{cr}^N$ is the critical value separating the *azimuthal-propagating* from the *azimuthal-evanescent* modes (i.e. terms decaying exponentially with respect to the index $m$) in $N$th ring. Then, an additional number of azimuthal terms is used, such as a satisfactory convergence of the pressure field to be achieved near the vicinity of the interfaces, where the maximum number of azimuthal terms is required.

The phenomenon which dominates the numerical calculations of the studied problem is that of exponential dichotomy: the solution contains both Hankel functions of the first and second kind. For a fixed order $m$ and large arguments, $H_m^{(1)}(\lambda_n r)$ decay exponentially, while $H_m^{(2)}(\lambda_n r)$ grow exponentially; that is forward and

backscattered energies are involved in the solution. Trying to resolve both rapidly growing and decaying waves over many wavelengths causes considerable numerical difficulties, which prompts for formulating the pressure field (11) and (12) with the normalized Hankel functions (15a) and (15b). This also indicates that wide cylindrical rings, except the inner and the outer, do not permit of a straightforward numerical treatment.

Similar comments have been made in a work presenting a coupled-mode solution for acoustic propagation in a cylindrically symmetric ocean with stepwise depth variations [8]. In that work, the environment is considered to be azimuthally symmetric with respect to the source and thus, only Hankel functions of zeroth order appear in the solution. The present study deals with a fully 3-D environment, which means that the pressure field strongly depends on the azimuth; the dependence is expressed in the solution by the order $m$ of the Hankel functions. This additional parameter increase the difficulty of the numerical calculations, which calls for a special treatment.

The nature of the numerical difficulties mentioned above is related to the recursive-type method used for solving the problem, which is quite analogous to the propagator matrix method, used in seismic wave propagation. Also, the present numerical stability problem is similar to the one encountered in seismic waves, when applying the Thomson–Haskell propagation matrix. This problem could be overcome offering extension of the applicability of the 3D obtained solution to higher frequencies by various techniques. One approach, proposed by Evans [25], is based on the decoupling of the coupled modes in the recursive-type method. Another possibility is through a direct global matrix approach for setting up the system of equations, as proposed by Schmidt [26] and Ricks and Schmidt [27] for solving radiation/scattering from spherically stratified shells and cylindrically layered shells, respectively. A detailed comparison of direct global matrix approach to propagation matrix approach can be found in Ref. [3]. An effective solution to this problem could also be obtained by extensive investigation of the interplay between the large order and the large argument asymptotic approximations of the Hankel functions. (See also Section 4 in Ref. [7]).

### 5.2. Examples

In underwater acoustic applications the transmission loss (TL) of a pressure field is often a more useful quantity than the pressure itself. Therefore, in this section, results concerning the transmission loss of the acoustic field are presented for a ''triple-ring scatterer'' environment, utilizing the matching conditions on the interfaces of all three types of cylindrical regions (inner cylinder—intermediate ring, two successive intermediate rings, last obstacle ring—surrounding water). In the present work, the transmission loss is defined as

$$\mathrm{TL} = -20\log\frac{P(\mathbf{r})}{P_0(|\mathbf{r}| = 1m)}, \tag{37}$$

where $P(\mathbf{r})$ is the pressure modulus at a distance $|\mathbf{r}|$ from the source, and $P_0(|\mathbf{r}| = 1m) = 1/4\pi$ is the modulus of the free-space Green's function at a distance of 1 m from the source. The values of the unaltered parameters configuring the geometry of the environment are chosen as follows: depth of the waveguide and height of the cylindrical scatterer $H = 250\,\mathrm{m}$, source depth $z_s = 50\,\mathrm{m}$, distance between source and axis of the cylindrical scatterer $r_s = 1000\,\mathrm{m}$, radii of the cylindrical rings of the scatterer $r_1 = 50\,\mathrm{m}$, $r_2 = 80\,\mathrm{m}$ and $r_3 = 100\,\mathrm{m}$.

Three cases corresponding to cylindrical obstacles with different acoustic structure (OBS1–OBS3) are demonstrated and compared. The composition (rings 1–3) of the scatterers is (moraine, hard, soft) for OBS1, (water, hard, soft) for OBS2 and (moraine, water, hard) for OBS3. The corresponding acoustic properties (sound speed $c$ in m/s, density $\rho$ in g/cm$^3$) of the materials are (1510, 1) for water, (1520, 1.4) for soft, (1677, 1.83) for hard and (1950, 2.1) for moraine. All the results presented in this section were obtained by using the depth-dependent sound-speed profile in water, $c_4(z)$, depicted in Fig. 2, and a corresponding density $\rho_4 = 1\ \mathrm{g/cm^3}$.

A low frequency of 10 Hz has been chosen for the acoustic source, the non-dimensional wavenumbers varying from $k_1r_1 = 1.61$ to $k_3r_3 = 4.13$. For this source frequency, corresponding to a wavelength of 152 m for $\max\{c_4(z)\} = 1520\,\mathrm{m/s}$, the effect of the depth variation of the sound speed profile $c_4(z)$ is not expected to be visible, while the scatterer with diameter $2 \times r_3 = 200\,\mathrm{m}$ will be perceptible by the acoustic waves. In order

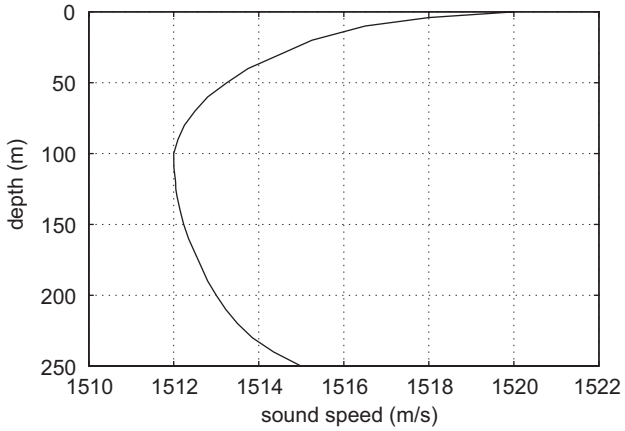


Fig. 2. The depth-dependent sound-speed profile used for the TL calculations.

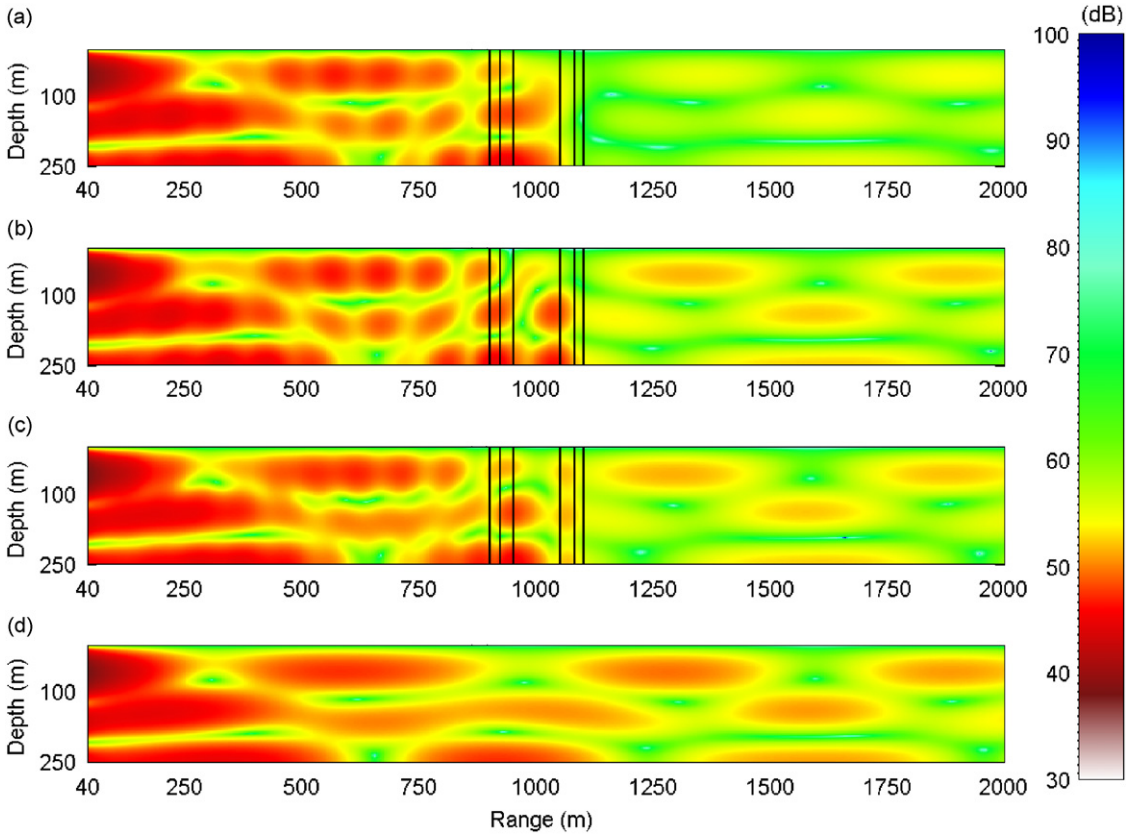


Fig. 3. TL at $f = 10\,\text{Hz}$ calculated on a vertical slice passing through the source and the axis of the obstacles. (a) OBS1, (b) OBS2, (c) OBS3, (d) without obstacle. The geometrical parameters of the environment are: waveguide depth $H = 250\,\text{m}$, source depth $z_s = 50\,\text{m}$, distance between source and axis of the cylindrical scatterer $r_s = 1000\,\text{m}$, radii of the cylindrical rings of the scatterer $r_1 = 50\,\text{m}$, $r_2 = 80\,\text{m}$ and $r_3 = 100\,\text{m}$.

to achieve satisfactory convergence for the pressure field a lower bound of 5 azimuthal terms was derived by imposing $m_{\max} > m_{cr}^N(n=1) = \lambda_1^N r_N$ (see Section 5.1) and 4–5 additional azimuthal terms (i.e. a total of 9–10) were finally used in the calculations.

In Figs. 3a–c, TL is presented on a vertical slice passing through the source and the axis of the cylindrical obstacles OBS1 (Fig. 3a), OBS2 (Fig. 3b) and OBS3 (Fig. 3c). In Fig. 3d, TL of the axisymmetric field in the unobstructed waveguide is presented. To comment on the figures more conveniently, the cross sections of the scatterer rings are called *columns* and ordered with respect to the distance from the source, $R$, starting from the insonified side of the scatterer; thus, the cross section of ring 3 from $R = 900$ to 920 m is the first column,

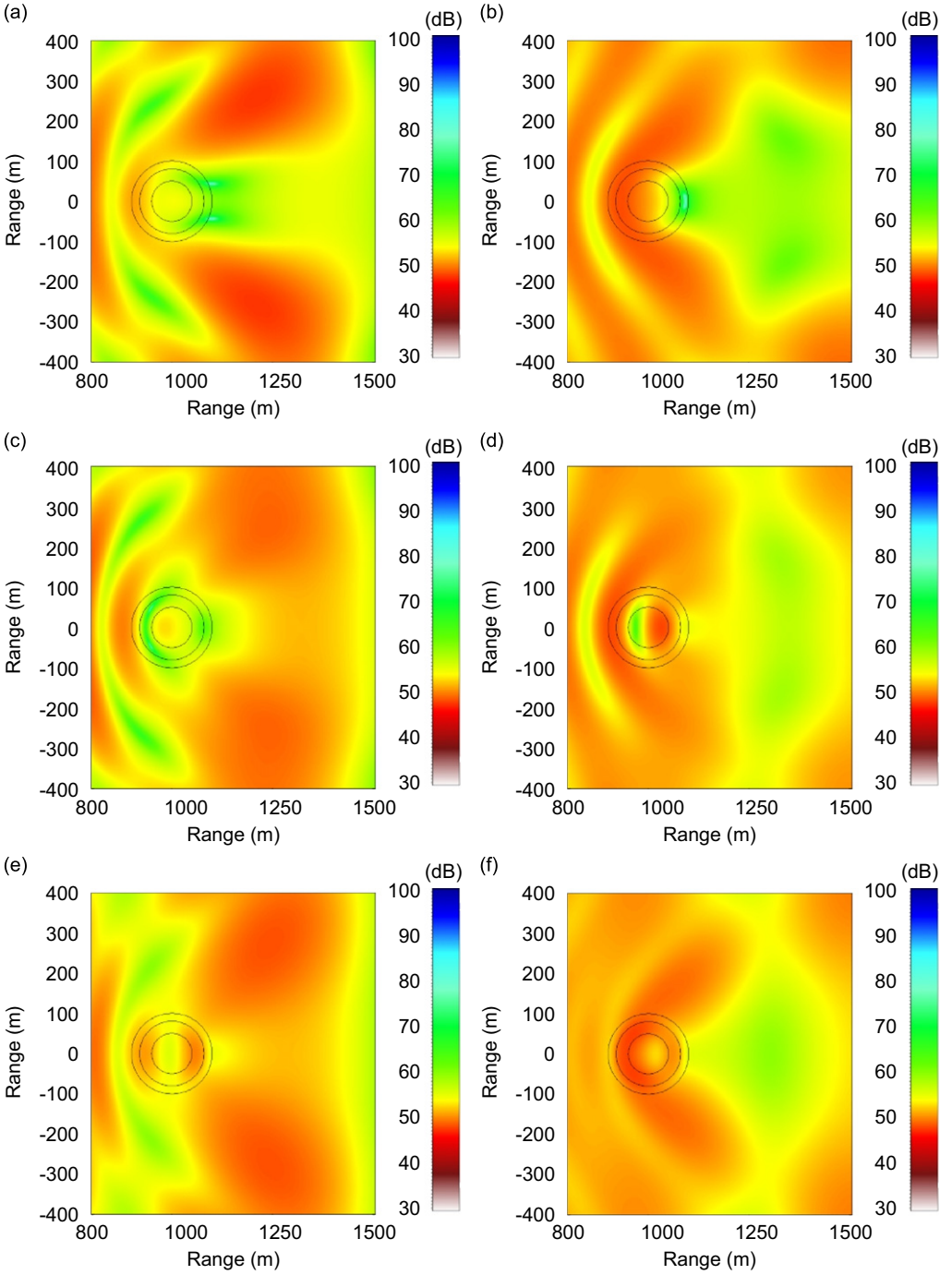


Fig. 4. TL at $f = 10$ Hz calculated on a horizontal plane passing through the source point for OBS1 (a,b), OBS2 (c,d) and OBS3 (e,f) at $z = 50$ m (a,c,e) and $z = 150$ m (b,d,f). The geometrical parameters of the environment as in Fig. 3.

the adjacent cross section of ring 2 from $R = 920$ to 950 m is the second column, etc., the cross section of ring 3 from $R = 1080$ to 1100 m is the last (fifth) column. The TL pattern in the insonified region up to about 750 m away from the source presents similarities in all four cases, while an oscillatory form of the TL patterns for the obstacle cases is observed due to the interaction of the incident and backscattered field. Similarities are also observed in the TL pattern for all the cases behind the obstacle; the TL level is highest for the OBS1-case and lowest for the case of the obstacle absence, as expected. The energy paths are not very well formed due to the low frequency of the source. The structure of OBS1 (Fig. 3a) causes trapping of energy in the first three columns, followed by a distinct shadow zone. As concerns OBS2 (Fig. 3b), shadow areas of high TL level are observed in the water core, an indication of energy absorption by the two first columns. Energy is trapped between the obstacle axis and the interface at 1080 m because of the backscattering from the last two columns. The sound seems to penetrate the last column and escape to the surrounding water mainly at depths from 120 to 150 m and secondarily close to the bottom of the waveguide. In OBS3 (Fig. 3c) the second water column allows a part of the acoustic energy to enter the very hard core, while an energy trapping is clearly observed in the fourth water column due to the blocking effect of the two adjacent hard columns.

In order to clearly demonstrate the 3D character of the acoustic field for the studied environment, TL graphs on a horizontal plane at depths (i) $z = 50$ m (the source depth) and (ii) $z = 150$ m are provided for the three different-structured obstacles OBS1, OBS2 and OBS3. In Figs. 4a–f, TL is presented in a frame 700 m × 800 m, extended 100 m in front and 400 m behind the center of the obstacles and placed symmetrically to the source–obstacle axis, i.e. the line connecting the source and the center of the obstacles. The expected symmetry of the acoustic field with respect to the source–obstacle axis is obviously observed. A common feature appearing in all figures is the side lobes of level 45–55 dB, varying in form and position with respect to the depth and the obstacle structure. The intense differences of the TL pattern on the $(r, \theta)$-plane around all three obstacles presented at the depths of 50 and 150 m reveal the complexity of the combined effect of the sound propagation and the multiple backscattering from the interfaces of penetrable scatterers with various acoustic properties.

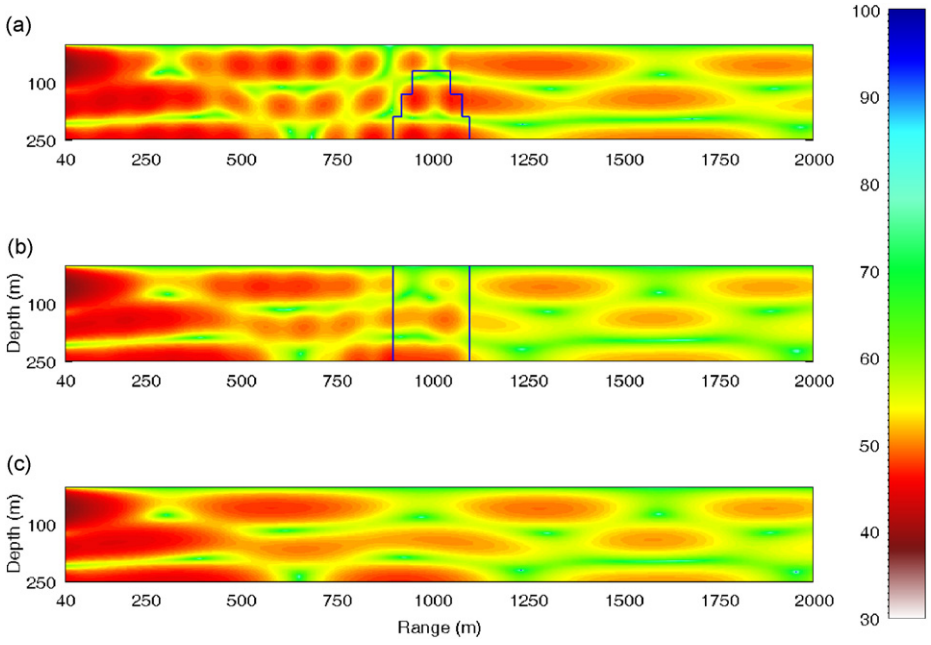


Fig. 5. TL at $f = 10$ Hz calculated on a vertical slice passing through the source and the axis of the cylindrical scatterers: (a) a soft seamount composed by three cylindrical rings of radii $r_1 = 50$ m, $r_2 = 80$ m and $r_3 = 100$ m (maximum radius), (b) a soft cylinder of radius $r_1 = r_2 = r_3 = 100$ m, modeling a steep cylindrical island, (c) without obstacle. The geometrical and physical parameters of the environment and the source data are the same as in Fig. 3.

The previous example, presented in Figs. 3 and 4, focuses on the study of azimuthal matching between the different modal series expansions of the acoustic field on the various subdomains, given by Eqs. (10)–(12), on the vertical interfaces (the cylindrical surfaces ranging from $z = 0$ to $H$) separating the latter ring-type subdomains. This particular example represents physically the case of 3D scattering by a multi-layered sharp island (with vertical walls) in the ocean acoustic waveguide.

In order to further demonstrate the applicability of our method to 3D acoustic scattering by more general axisymmetric obstacles, we present in Fig. 5a the scattering field by a soft seamount in the same as before waveguide, as obtained by the present method. Again, the incident field is generated by a harmonic point source with frequency 10 Hz, located at 50 m depth (below the free surface). The present axisymmetric obstacle represents a homogeneous soft seamount-type obstacle, with density $\rho = 1.4\,\mathrm{g/cm^3}$ and sound speed $c = 1520\,\mathrm{m/s}$, modelled as a three-ring element with radii $r_1 = 50\,\mathrm{m}$, $r_2 = 80\,\mathrm{m}$, $r_3 = 100\,\mathrm{m}$ (maximum radius), and vertical discontinuity (stratification) at the depths of 70, 130, and 190 m, respectively; see Fig. 5a. For comparison, we present in Fig. 5b the scattering field by a homogeneous soft vertical cylinder extending from the top to the bottom of the same waveguide, located at the same position and having the same maximum radius. Also, in Fig. 5c the propagation in the same unobstructed waveguide is presented. We clearly observe in this figure that, on the plane passing through the point source and the centerline of the scatterers, the seamount permits the radiation of more acoustic energy in the downwave direction than the vertical island, which blocks the energy on this plane as it is naturally expected. This fact is especially true at the top part of the waveguide (depths less than 70 m) that remains unobstructed in the case of the seamount.

## 6. Conclusions

In this paper acoustic field computations for the problem of 3D scattering from a penetrable radially layered cylindrical obstacle in a shallow-water environment are presented using coupled-mode series expansions of the pressure field. Exploitation of the matching conditions on the cylindrical interfaces results in an infinite linear system for the expansion coefficients. The system is appropriately truncated and numerically solved. Results concerning the transmission loss outside and inside obstacles, consisting of three cylindrical rings, are given for a typical depth-dependent ocean sound-speed profile. The non-dimensional wavenumbers $kr_j$ vary from about 1.5 to 4, where $r_j$ is the radius of the $j$ ring of the cylindrical obstacle.

Since the presented solution considers multi-layered cylindrical scatterers (both in the vertical and radial direction), it could serve as a benchmark for modeling 3D acoustic scattering from sufficiently realistic axisymmetric inhomogeneities in ocean waveguides. Examples of problems dealing with 3D acoustic scattering in ocean waveguides, which can be treated using the analysis presented herein, are the scattering from (i) cylindrical obstacles with quasi-continuous variation of the acoustic properties, (ii) a group of cylindrical discs with the same axis of symmetry and radial variation of sound speed and density, (iii) an axisymmetric obstacle with a fluid-filled cavity, and (iv) a cylindrically symmetric eddy or a cylindrically symmetric bathymetric feature such as a seamount. Although the assumptions of an ideal free-surface and ideal bottom boundaries have been made in this work, the solution can be extended to penetrable ocean waveguides by replacing only the eigenvalues and eigenfunctions of the vertical eigenvalue problems with new ones, calculated by appropriate techniques.

As concerns the directions of future work, additional research effort can be further spent on the azimuthal convergence of the double series expressing the scattered field outside the obstacle and the total field inside the obstacle, as well as on the systematic investigation of the multi-parametric character of the problem. Furthermore, the applicability of the coupled-mode solution could be extended to higher frequencies by (i) controlling the phenomenon of exponential dichotomy, i.e. the involvement of waves simultaneously decaying and growing with range in the solution, which causes numerical difficulties on handling higher frequencies over distances extending to many wavelengths (this could be achieved using various techniques/approaches such as decoupling algorithm [25] or a direct global matrix approach [26]); (ii) a detailed investigation of combined large-order and large-argument asymptotic approximations of the Hankel functions. Some of these enhancements are currently under study.

## Appendix. Verification of present analysis by means of a simplified case

Let us consider the environment of Section 2 with $N=3$, assume that the three $(c,\rho)$-profiles are constant and set $c_1(z)=c_b$, $\rho_1(z)=\rho_b$, $c_3(z)=c_2(z)=c_w$ and $\rho_3(z)=\rho_2(z)=\rho_w$. This actually means that the cylindrical interface at $r_2$ is an artificial one.

For the environment described above, it will be shown that (i) expression (10) for the pressure field in the inner ring is identical with Eq. (9), corresponding to the pressure field inside a single penetrable cylindrical obstacle, and (ii) expressions (11) and (12) for the pressure field in rings 2 and 3, respectively, are identical with Eq. (6), corresponding to the pressure field in the water surrounding a single penetrable cylindrical obstacle.

The following relations have to be taken into account in the algebraic manipulations:

$$J_m(x)=\frac{H_m^{(1)}(x)+H_m^{(2)}(x)}{2}, \tag{38a}$$

$$\mathscr{W}\{H_m^{(1)}(x),H_m^{(2)}(x)\}=-\frac{4i}{\pi x}, \tag{38b}$$

$$\mathscr{W}\{H_m^{(1)}(x),J_m(x)\}=-\mathscr{W}\{H_m^{(2)}(x),J_m(x)\}=-\frac{2i}{\pi x}, \tag{38c}$$

where $\mathscr{W}$ is the symbol of the Wronskian.

Also, Graf's addition theorem (see Eq. (17)) is used for transforming the axisymmetric field in the unobstructed waveguide $p_i$ (see Eq. (12)) into a double series expansion.

In the case of an isovelocity environment, as the one studied here, the coupling coefficients (22a) and (22b) are vanished for $n\neq v$. Consequently, Eqs. (26a), (26b) and Eqs. (29a), (29b) take the form

$$\begin{aligned} A_{vm}^1 &= \mathscr{E}_{nm}^{\mathrm{I},1}(a)A_{nm}^2+\mathscr{E}_{nm}^{\mathrm{II},1}(a)B_{nm}^2,\\ 0 &= \mathscr{E}_{nm}^{\mathrm{III},1}(a)A_{nm}^2+\mathscr{E}_{nm}^{\mathrm{IV},1}(a)B_{nm}^2, \end{aligned} \tag{39}$$

and

$$\begin{aligned} A_{nm}^2 &= \mathscr{E}_{nm}^{\mathrm{I},2}(b)A_{nm}^3+\mathscr{E}_{nm}^{\mathrm{II},2}(b)B_{nm}^3,\\ B_{nm}^2 &= \mathscr{E}_{nm}^{\mathrm{III},2}(b)A_{nm}^3+\mathscr{E}_{nm}^{\mathrm{IV},2}(b)B_{nm}^3, \end{aligned} \tag{40}$$

respectively. Given that $\lambda_n^2=\lambda_n^3=\lambda_n$, and setting $\gamma=\rho_w/\rho_b$, $\mu_n=\lambda_n^1$, $a_n^1=\mu_n a$, $a_n^2=\lambda_n a$ and $b_n=\lambda_n b$, the coefficients $\{\mathscr{E}_{nm}^{i,j}, i=\mathrm{I},\ldots,\mathrm{IV},\ j=1,2\}$, the general form of which is given in Section 4, are expressed as follows:

$$\mathscr{E}_{nm}^{\mathrm{I},1}(a)=\sqrt{\gamma}\frac{H_m^{(1)}(a_n^2)}{H_m^{(1)}(b_n)},$$

$$\mathscr{E}_{nm}^{\mathrm{II},1}(a)=\sqrt{\gamma}\frac{H_m^{(2)}(a_n^2)}{H_m^{(2)}(b_n)},$$

$$\mathscr{E}_{nm}^{\mathrm{III},1}(a)=-\frac{D_{nm}^{(1)}}{\sqrt{\gamma}a_n^1H_m^{(1)}(b_n)J_m'(a_n^1)},$$

$$\mathscr{E}_{nm}^{\mathrm{IV},1}(a)=-\frac{D_{nm}^{(2)}}{\sqrt{\gamma}a_n^1H_m^{(2)}(b_n)J_m'(a_n^1)},$$

$$\mathscr{E}_{nm}^{\mathrm{I},2}(b)=1,$$

$$\mathscr{E}_{nm}^{\mathrm{II},2}(b)=\frac{\sigma}{2}H_m^{(1)}(b_n),$$

$$\mathscr{E}_{nm}^{\mathrm{III},2}(b) = 0,$$

$$\mathscr{E}_{nm}^{\mathrm{IV},2}(b) = \frac{\sigma}{2} H_m^{(2)}(b_n), \tag{41}$$

where

$$D_{nm}^{(\ell)} = a_n^2 J_m(a_n^1) H_m^{(\ell)\prime}(a_n^2) - \gamma a_n^1 J'_m(a_n^1) H_m^{(\ell)}(a_n^2), \quad \ell = 1,2 \tag{42}$$

and

$$\gamma = \rho_w/\rho_b, \quad \sigma = \frac{i}{4\rho(z_s)}. \tag{43}$$

Using expressions (41) for $\mathscr{E}$-coefficients and given that $B_{nm}^3 = 1$ (see Eq. (33b)), we obtain

$$A_{nm}^1 = -\frac{\sqrt{\gamma}}{2\pi\rho_w D_{nm}^{(1)}} J_m(a_n^1), \tag{44a}$$

$$A_{nm}^2 = -\frac{\sigma}{2} H_m^{(1)}(b_n) \frac{D_{nm}^{(2)}}{D_{nm}^{(1)}}, \tag{44b}$$

$$A_{nm}^3 = \sigma H_m^{(1)}(b_n) \frac{D_{nm}^J}{D_{nm}^{(1)}}, \tag{44c}$$

$$B_{nm}^2 = \frac{\sigma}{2} H_m^{(2)}(b_n), \tag{44d}$$

where

$$D_{nm}^J = a_n^2 J_m(a_n^1) J'_m(a_n^2) - \gamma a_n^1 J'_m(a_n^1) J_m(a_n^2). \tag{45}$$

Introducing expression (44a) into Eq. (10), and setting $g_n^1(z) = \psi_n(z)$, we obtain the pressure field $p_1$ in the inner cylinder of the obstacle

$$p_1 = -\sum_{n=1}^{\infty}\sum_{m=0}^{\infty} e_m d_{s,nm} \left[\frac{\sqrt{\gamma}}{2\pi\rho_w D_{nm}^{(1)}}\right] J_m(\mu_n r)\psi_n(z)\cos m\theta, \tag{46}$$

which, taking into account Eq. (14), is found to be identical with the pressure field inside a single cylindrical obstacle, given by Eq. (9).

Similarly, introducing expressions (44b), (44d) into Eq. (11) and Eq. (44c) into Eq. (12), and setting $g_n^2(z) = g_n^3(z) = g_n(z)$, we obtain the pressure fields in the outer cylindrical ring of the obstacle, $p_2$, and the surrounding water, $p_3$,

$$p_2 = -\frac{\sigma}{2}\sum_{n=1}^{\infty}\sum_{m=0}^{\infty} e_m d_{s,nm} \left[\frac{D_{nm}^{(2)}}{D_{nm}^{(1)}} H_m^{(1)}(\lambda_n r) - H_m^{(2)}(\lambda_n r)\right] g_n(z)\cos m\theta, \tag{47}$$

$$p_3 = p_i - \sigma\sum_{n=1}^{\infty}\sum_{m=0}^{\infty} e_m d_{s,nm} \frac{D_{nm}^J}{D_{nm}^{(1)}} H_m^{(1)}(\lambda_n r) g_n(z)\cos m\theta. \tag{48}$$

After some algebra, the coefficients $A_{nm}^{sc}$ in Eq. (7) can be expressed as

$$A_{nm}^{sc} = -\sigma \frac{D_{nm}^J}{D_{nm}^{(1)}}. \tag{49}$$

Introducing Eq. (49) into Eq. (6), it is proved that the pressure field given by Eq. (6), is identical with the pressure field in the surrounding water $p_3$, as expected.

Finally, making appropriate algebraic manipulations, we result in $p_2 \equiv p_3$.

## References


[1] M.J. Buckingham, Ocean-acoustic propagating models, *Journal d'Acoustique* (1992) 223–287.

[2] J.S. Papadakis, Ocean acoustic models for low frequency propagation in 2D and 3D environments, *Acustica-Acta Acustica* 84 (1998) 1031–1041.

[3] F.B. Jensen, W.A. Kuperman, M.B. Porter, H. Schmidt, *Computational Ocean Acoustics*, AIP Press, American Institute of Physics, New York, 1994.

[4] D. Lee, M.H. Schultz, *Numerical Ocean Acoustic Propagation in Three Dimensions*, World Scientific, Singapore, 1995.

[5] G.A. Athanassoulis, A.M. Prospathopoulos, Three-dimensional acoustic scattering of a source-generated field from a cylindrical island, *Journal of the Acoustical Society of America* 100 (1996) 206–218.

[6] G.A. Athanassoulis, K.A. Belibassakis, D.A. Mitsoudis, D.A. Kampanis, V.A. Dougalis, Coupled mode and finite element approximations of underwater sound propagation problems in general stratified environments, *Journal of Computational Acoustics* 16 (2008) 83–116.

[7] R.B. Evans, Three dimensional acoustic scattering from a cylindrical inclusion in a waveguide, in: D. Lee, A. Cacmak, R. Vichnevetsky (Eds.), *Computational Acoustics*, Vol. 2, North-Holland, Amsterdam, 1990, pp. 123–132.

[8] R.B. Evans, A coupled mode solution for acoustic propagation in a waveguide with stepwise depth variations of a penetrable bottom, *Journal of the Acoustical Society of America* 74 (1983) 188–195.

[9] S. Strange, W. Friederich, Guided wave propagation across sharp lateral heterogeneities the complete wavefield at a cylindrical inclusion, *Geophysics Journal International* 111 (1992) 470–482.

[10] G.A. Athanassoulis, A.M. Prospathopoulos, 3D acoustic scattering of source-generated acoustic field by an axisymmetric island, in: Z. Jagodzinski, R. Salamon (Eds.), *Proceedings of the XIth Symposium on Hydroacoustics*, Gdynia-Jurata, Poland, The Academy of Polish Navy, 1994, pp. 75–82.

[11] M.I. Taroudakis, A coupled-mode formulation for the solution of the Helmholtz equation in water in the presence of a conical seamount, *Journal of Computational Acoustics* 4 (1996) 101–121.

[12] J.A. Fawcett, Coupled-mode modeling of acoustic scattering from three-dimensional, axisymmetric objects, *Journal of the Acoustical Society of America* 102 (1997) 3387–3393.

[13] G.A. Athanassoulis, K.A. Belibassakis, Th. Gerostathis, A coupled-mode theory for the scattering of the acoustic waves from localized 3D scatterers superimposed over a parallel-contour bathynetry, in: P. Chevret, M.E. Zakharia (Eds.), *Proceedings of the 5th European Conference on Underwater Acoustics*, Lyon, France, European Communities, Luxembourg, 2000, p. 9.

[14] R.B. Evans, Stepwise coupled mode scattering of ambient noise by a cylindrically symmetric seamount, *Journal of the Acoustical Society of America* 119 (2006) 161–167.

[15] J.A. Fawcett, Modeling scattering from azimuthally symmetric bathymetric features using wavefield superposition, *Journal of the Acoustical Society of America* 122 (2007) 3286–3295.

[16] M.J. Buckingham, Theory of acoustic propagation around a conical seamount, *Journal of the Acoustical Society of America* 80 (1986) 265–277.

[17] T.K. Berger, Theory of acoustic radiation near a hyperbolic ridge, *Journal of the Acoustical Society of America* 104 (1998) 2136–2148.

[18] G.A. Athanassoulis, A.M. Prospathopoulos, Three-dimensional acoustic scattering from a penetrable layered cylindrical obstacle in a horizontally stratified ocean waveguide, *Journal of the Acoustical Society of America* 107 (2000) 2406–2417.

[19] L.-W. Cai, D.K. Dacol, D.C. Calvo, G.J. Orris, Acoustical scattering by arrays of cylinders in waveguides, *Journal of the Acoustical Society of America* 122 (2007) 1340–1351.

[20] G.A. Athanassoulis, A.M. Prospathopoulos, K.A. Belibassakis, A normal-mode solution for 3D acoustic scattering from a cylindrical island, in: J.A. Papadakis (Ed.), *Proceedings of the 3rd European Conference on Underwater Acoustics*, FORTH, Heraklion, Hellas, 24–28 June, Crete University Press, Heraklion, 1996, pp. 273–278.

[21] G.A. Athanassoulis, K.A. Belibassakis, All-frequency normal-mode solution of the three-dimensional acoustic scattering field from a cylindrical obstacle in a waveguide, *Journal of the Acoustical Society of America* 101 (1997) 3371–3384.

[22] H. Überall, R.D. Doolittle, J.V. McNicholas, Use of sound pulses for a study of circumferential waves, *Journal of the Acoustical Society of America* 39 (1966) 564–578.

[23] A. Zinoviev, Application of the Multi-Modal Integral Method (MMIM) to Sound Wave Scattering in an Acoustic Waveguide, PhD Thesis, Department of Mechanical Engineering, University of Adelaide, 1999.

[24] M. Abramowitz, I.A. Stegun, *Handbook of Mathematical Functions*, ninth ed., Dover Publications, New York, 1972.

[25] R.B. Evans, The decoupling of stepwise coupled modes, *Journal of the Acoustical Society of America* 80 (1986) 1414–1418.

[26] H. Schmidt, Numerically stable global matrix approach to radiation and scattering from spherically stratified shells, *Journal of the Acoustical Society of America* 94 (1993) 2420–2430.

[27] D.C. Ricks, H. Schmidt, A numerically stable global matrix method for cylindrically layered shells excited by ring forces, *Journal of the Acoustical Society of America* 95 (1994) 3339–3349.